Dynamics of an electrically charged polymer jet

Subbotin, A.; Stepanyan, R.; Chiche, A.; Slot, J. J. M.; ten Brinke, G.

Published in:
Physics of Fluids

DOI:
10.1063/1.4824109

PHYSICS OF FLUIDS **25**, 103101 (2013)

Dynamics of an electrically charged polymer jet

A. Subbotin,[1,2,a)] R. Stepanyan,[3] A. Chiche,[3] J. J. M. Slot,[3,4] and G. ten Brinke[2]

[1]*A.V. Topchiev Institute of Petrochemical Synthesis, Russian Academy of Sciences, Moscow 119991, Russia*
[2]*Department of Polymer Chemistry and Zernike Institute for Advanced Materials, University of Groningen, Nijenborgh 4, 9747 AG Groningen, The Netherlands*
[3]*Materials Science Centre, DSM Research, P.O. Box 18, 6160 MD Geleen, The Netherlands*
[4]*Department of Mathematics and Computer Science, Technische Universiteit Eindhoven, P.O. Box 513, 5600 MB Eindhoven, The Netherlands*

(Received 16 April 2013; accepted 14 September 2013; published online 10 October 2013)

Electro-hydrodynamic equations describing the behavior of a charged polymer jet are analyzed by analytical methods and scaling approach. A FENE-P constitutive equation is employed to describe the viscoelastic properties of a conducting polymer liquid. Effects of the electric field, the flow rate, and the material parameters on the jet dynamics are investigated. Four different regimes are examined. In particular, a regime in which the electric current is linearly proportional to the electric field and independent on the flow rate and a regime in which the electric current is linearly proportional to the flow rate and independent on the electric field are identified. An operating window limiting the region of a stable cone-jet mode is also considered. [http://dx.doi.org/10.1063/1.4824109]

I. INTRODUCTION

Electrospinning of polymeric solutions is a simple and relatively effective method for production of nanofibers and non-woven structures based on them. Since the process has regained interest in 1990s, the growing amount of experimental publications is devoted to its various aspects, mainly such as spinnability of different polymers and the correlation between the process and the material parameters on the one hand and the fiber diameter on the other.[1–6] At the same time, one of the main disadvantages of electrospinning disallowing its vast acceptance in the industry is the limited production rate: a typical highest achievable solution throughput varies between 1 ml/h and 10 ml/h rendering the process useless for large scale production. Different workarounds have been proposed, including the multi-nozzle process and electrospinning from a free liquid surface.[7,8] However, as a systematic fundamental knowledge of the factors limiting stable operation is still lacking, little progress can be made in tuning the material parameters not only to obtain certain fiber diameter range but also to increase the productivity and make the process more feasible for the industry. Hence, one of the challenging problems in the field is an optimization of the electrospinning process and understanding how different governing parameters influence the jet dynamics and stability as well as the fiber diameter.

In general, an electrospinning setup consists of a nozzle (a needle or a protruding opening in the upper electrode) and a counter electrode, as depicted in Figure 1. Although the solution flow rate Q and the electric field E can be controlled independently, via a syringe pump and a high voltage generator, respectively, in reality a long term stationary electrospinning process can be achieved only in a small region in the (E, Q) plane. Unfortunately, the electrospinning literature lacks systematic investigation of the steady operation window although there is evidence that it can be quite narrow.[6] On the other hand, different operation regimes in *electrospraying* have been studied more thoroughly:

[a)]Electronic mail: subbotin@ips.ac.ru

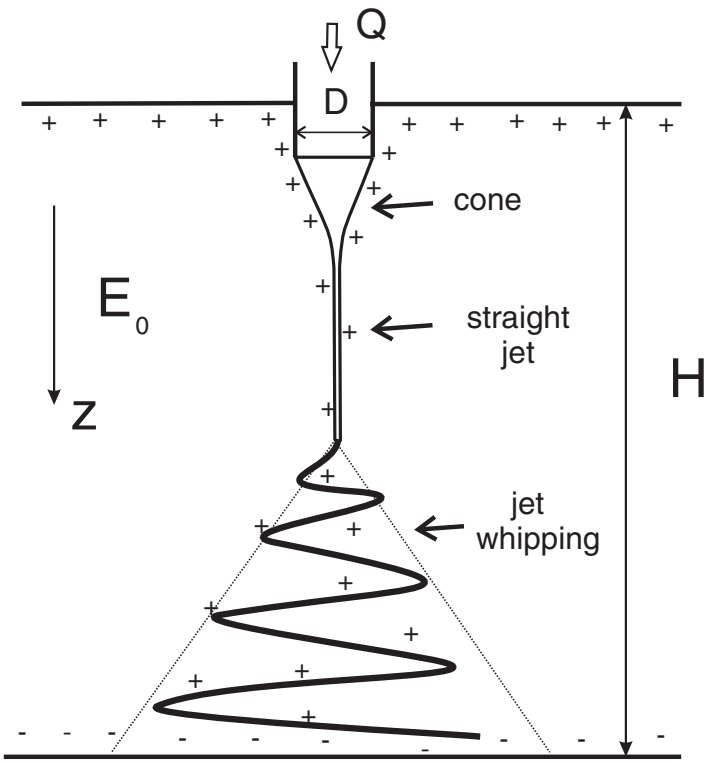

FIG. 1. Schematic picture of the jet formation.

e.g., Cloupeau and Prunet-Foch[9] have shown that the steady operation region shape and dependence on the material parameters is far from trivial.

Stability and dynamics of the electrospinning jet depends on the intricate interplay of surface tension, electric forces and rheology of the polymeric solution, although sometimes it is also affected by gravity and inertial effect. There has been some progress made in understanding how different factors influence the jet dynamics. General electro-hydrodynamic equations of an electrified liquid jet have been formulated[10–13] in the framework of a so-called leaky dielectric model.[14] However, their direct numerical solution is of limited use for electrospinning as it is profoundly difficult due to large disparity of the length scales involved and can be obtained only in a narrow range of parameter values.[15,16] Moreover, as the physics in such an approach is very much hidden underneath heavy numerics, limited qualitative insight can be gained. Simplifications, such as reducing the problem to one dimension, are often applied[17–19] but introduce inconsistencies: e.g., the electric current cannot be calculated anymore and has to be treated as an input parameter. Among others, the effects of viscoelasticity[20,21] and the axisymmetric and bending instability[17] have been studied in the framework of such an approach for the initial part of an electrospun jet.

An alternative approach, often applied in the modeling of electrospraying,[11,22] is a scaling analysis. It allowed the identification and classification of different electrospraying regimes[11] and prediction of their domains in the parameter space. Also, certain universal trends observed in electrospraying experiments were successfully predicted, the most known example of which is the electric current being independent on the voltage but scaling as a square root of the flow rate.[11,23] A similar approach being applied to electrified jets emitted in a cone-jet mode, also relevant for electrospinning,[12,24] resulted in scaling relations for the electric current, jet diameter and length of the cone-jet transition zone. Two different regimes – viscosity and surface tension dominated – were identified based on the relative importance of the corresponding forces. In contrast to electrospraying, the electric current I has been shown to depend both on the flow rate Q and the electric field E, yielding scaling relations $I \sim \eta^{1/6} K^{1/2} E^{2/3} Q^{2/3}$ for viscous and $I \sim \alpha^{2/7} K^{3/7} E^{3/7} Q^{4/7}$ for capillary regimes, where η, α, and K denote liquid viscosity, surface tension, and electric

conductivity, respectively. Also in this approach only a Newtonian liquid has been considered and the throughput and the electric field have been treated as completely independent parameters implying that no predictions on the stable operation window have been made. On the other hand, experiments show[1–6] the electric current to be very insensitive to the throughput and viscoelastic effects to be essential.

Apart from the technological relevance, the problem about the highest and the lowest achievable flow rates is of a great scientific interest.[22] For instance, the finest diameters of the fibers in electrospinning or the smallest droplets in electrospraying are obtained when the applied flow rates are reduced to a minimum. An existence of such a limiting rate is in some cases explained by a complete charge separation – saturation of the number of available charge carriers. However, in the majority of cases, especially for highly conductive liquids, the minimum attainable rates are still far beyond the complete charge separation limit rendering such an explanation invalid.[22] To our knowledge, no consistent theory explaining the existence of a minimal flow rate has been formulated to this date.

To summarize, although considerable progress in the understanding of the electrospinning process has been achieved during the past 20 years, there is still a number of problems, which have not received enough theoretical attention yet. One of the most important of them is the prediction of the stationary operation region in the (E, Q) plane. Also the influence of viscoelasticity on the electrospinning regimes and their boundaries has received relatively little attention.

In the present work the dynamics of an electrified jet formed in an electrospinning process is analyzed. Starting from the general electro-hydrodynamic equations, formulated in Sec. II, analysis of electrospinning regimes is performed in Sec. III in order to identify the influence of the material properties, especially viscoelasticity, and the process parameters on the jet characteristics. Special attention is paid to the boundaries of the stationary operating window, in Sec. IV.

II. MODEL AND BASIC EQUATIONS

We assume that the electrically conducting polymer solution is pumped at a flow rate Q out of an orifice with diameter D located at the top electrode, Fig. 1. The electrodes generate homogeneous electric field of strength E_0 directed along the z-axis and coinciding with the direction of the gravity force. The distance between the electrodes is equal to H, at that $H \gg D$. As experimental observations[1–6, 22] show, a charged liquid cone is formed at the orifice and then transformed into a thin straight jet. Later on the jet becomes unstable with respect to whipping, Fig. 1.

The polymer solution is characterized by its density ρ, electrical conductivity K, dielectric constant ε, and surface tension α. We do not consider the exact nature of the charges in the solution but assume the polymer is carrying charges of the same sign as the upper electrode – positive – due to ionization. For the surrounding gas medium we assume that $\rho = K = 0$ and $\varepsilon = 1$. Additional parameters are connected with the polymeric nature of the liquid. A polymer chain has a contour length L and a Kuhn segment length a, so that the number of segments per chain is $N = L/a$. Concentration of the polymer chains in solution equals to n and the relaxation time is τ. Using above parameters we can define the elastic modulus $G \simeq nk_BT$, and the linear viscosity $\eta \simeq G\tau$ of the polymer solution.[25,26] As a simple estimation shows, a typical value of τ for the polymer solutions used in electrospinning is $\tau \sim 10^{-5} \div 10^{-1}$ s.

The behavior of the electrospun polymer liquid can be described by a set of electro-hydrodynamic equations, which include the momentum and the constitutive equation for the polymer solution and the charge relaxation equation on the free boundary. In order to formulate these equations we introduce the surface charge density σ, the electric field vector inside the fluid $\mathbf{E}(\mathbf{x}, t)$ and the velocity field $\mathbf{v}(\mathbf{x}, t)$.

A. Momentum equation

The general form of the momentum equation is given by

$$\rho \frac{\partial \mathbf{v}}{\partial t} + \rho \mathbf{v} \cdot \nabla \mathbf{v} - \nabla \cdot (\boldsymbol{\Sigma} - p\mathbf{I}) - \rho \mathbf{g} - q\mathbf{E} = 0, \tag{1}$$

where the velocity $\mathbf{v}(\mathbf{x}, t)$ obeys the incompressibility condition $\nabla \cdot \mathbf{v} = 0$. Here p is the pressure, ∇ is the gradient operator, $\boldsymbol{\Sigma}$ is the viscoelastic stress tensor, $\rho\mathbf{g}$ is the gravity force density, and $q\mathbf{E}$ is the electric force density (q is the free charge density). The differential equation (1) should be supplemented by appropriate boundary conditions on the free surface. These conditions imply the balance of the viscoelastic, capillary and electric forces

$$-p_s\mathbf{n} + \boldsymbol{\Sigma} \cdot \mathbf{n} + \alpha C\mathbf{n} - \mathbf{F} = 0, \tag{2}$$

where p_s is the pressure at the surface, $\mathbf{n}$ is a normal vector to the surface, $C = \operatorname{div}\mathbf{n}$ is the mean surface curvature, and $\mathbf{F}$ is the electric force per unit area.

Further on we use a cylindrical system of coordinates (z, r, φ) and assume that the cone and the jet surface is described by an axisymmetric function $r = r(z, t)$ so that the vectors normal and tangential to the surface are, respectively,

$$\mathbf{n} = -\frac{r_z'}{\sqrt{1+r_z'^2}}\mathbf{e}_z + \frac{1}{\sqrt{1+r_z'^2}}\mathbf{e}_r, \quad \boldsymbol{\tau} = \frac{1}{\sqrt{1+r_z'^2}}\mathbf{e}_z + \frac{r_z'}{\sqrt{1+r_z'^2}}\mathbf{e}_r.$$

In what follows we neglect the gravity force and assume that the Debye radius is small with respect to the jet diameter. The last condition implies that the charges are located in a thin surface layer with a thickness of the order of the Debye length and the bulk of the liquid is electrically neutral (in Eq. (1) $q = 0$). The coupling between the hydrodynamic and the electrostatic problem is due to the force acting on the surface of the jet. Per unit area, it reads[27,28]

$$\mathbf{F} \simeq \sigma E_\tau \boldsymbol{\tau} + \left(\frac{\sigma^2}{2\varepsilon_0} + \frac{\varepsilon_0(\varepsilon-1)}{2}E_\tau^2\right)\mathbf{n}, \tag{3}$$

where $E_\tau = \mathbf{E} \cdot \boldsymbol{\tau}$, $E_n = \mathbf{E} \cdot \mathbf{n}$.

The momentum equation (1) can be simplified using a slender body approximation, $|r_z'| < 1$ and the potentiality flow condition implying $\mathbf{v} \cdot \nabla\mathbf{v} = \frac{1}{2}\nabla \mathrm{v}^2$. After integration over the jet section $[z, z + dz]$ this equation is recast in a one-dimensional form

$$2\pi \int_0^{r(z,t)} r dr \rho \frac{\partial \mathrm{v}_z}{\partial t} + \frac{\partial}{\partial z}\left[2\pi \int_0^{r(z,t)} r dr \left(\frac{\rho \mathrm{v}_z^2}{2} + p - \Sigma_{zz}\right)\right] + 2\pi r\sqrt{1+r_z'^2}(p_s\mathbf{I} - \boldsymbol{\Sigma}) \cdot \mathbf{n}\mathbf{e}_z = 0. \tag{4}$$

Using the boundary condition (2) and defining the surface velocity in the normal direction as $\mathrm{v}_n = \mathbf{n} \cdot \mathbf{e}_r \frac{\partial r}{\partial t}$ we arrive to the final equation

$$\frac{\partial}{\partial t}\left(\rho r^2 \mathrm{v}_z\right) + r^2 \frac{\partial}{\partial z}(\alpha C - F_n) + \frac{\partial}{\partial z}\left[r^2\left(\frac{\rho \mathrm{v}_z^2}{2} + \Sigma_{nn} - \Sigma_{zz}\right)\right] \simeq 2rF_\tau. \tag{5}$$

The incompressibility condition $\nabla \cdot \mathbf{v} = 0$ reduces to the mass conservation equation $\frac{\partial r^2}{\partial t} + \frac{\partial}{\partial z}\left(r^2 \mathrm{v}_z\right) = 0$. Equation (5) has been derived in Refs. 17 and 19 using another methods.

B. Constitutive equation

Special attention has to be paid to the constitutive equation describing the polymer solution. In order to capture the viscoelastic effects, also in a strong elongational flow, we choose to approximate the rheology of the solution by a FENE-P model.[25,26] This model is appropriate to describe the rheological behavior of Boger fluids. It is formulated in terms of a conformation tensor $\mathbf{A} = \langle \mathbf{RR} \rangle$ where $\mathbf{R}$ is a polymer chain end-to-end distance and the angular brackets denote averaging. At equilibrium, $\langle \mathbf{R}^2 \rangle_0 \simeq aL \simeq a^2 N$. If one assumes that the stress tensor $\boldsymbol{\Sigma}$ is mainly determined by the polymer component, then in the framework of FENE-P one has

$$\boldsymbol{\Sigma} = G\frac{\mathbf{A}/R_0^2 - \mathbf{I}}{1 - \mathrm{tr}\mathbf{A}/L^2} \tag{6}$$

with $\mathbf{A}$ obeying

$$\tau\left[\frac{\partial \mathbf{A}}{\partial t}+(\mathbf{v}\cdot\nabla)\mathbf{A}-(\nabla\mathbf{v})^{T}\cdot\mathbf{A}-\mathbf{A}\cdot\nabla\mathbf{v}\right]+\frac{\mathbf{A}-R_0^2\mathbf{I}}{1-\mathrm{tr}\mathbf{A}/L^2}=0, \tag{7}$$

where

$$(\nabla\mathbf{v})_{ij}=\frac{\partial \mathrm{v}_j}{\partial x_i},\quad (\nabla\mathbf{v})^{T}_{ij}=\frac{\partial \mathrm{v}_i}{\partial x_j},\quad i,j=1,2,3$$

and $R_0^2=\frac{1}{3}\langle\mathbf{R}^2\rangle_0$. The FENE-P model contains three parameters: the elastic modulus G, the relaxation time τ, and the contour length L introduced to account for the finite extensibility of polymer chains. The linear viscosity of the polymer solution is expressed by means of the scaling relation $\eta\simeq G\tau$.

The components of the stress tensor can be found from Eqs. (6) and (7). We restrict ourselves to the steady elongation flow characterized by a strain rate $\dot{\varepsilon}$ as this situation is the most appropriate for the jet dynamics.[29,30] The flow rate and the strain rate in that case are presented as follows:

$$\mathrm{v}_z=\frac{Q}{\pi r^2(z)},\quad \dot{\varepsilon}=\frac{d\mathrm{v}_z}{dz}\simeq-\frac{Qr_z'}{r^3}. \tag{8}$$

For further analysis we identify three steady flow regimes corresponding to different stress behavior. If $\dot{\varepsilon}\tau\ll 1$, the conformations of the polymer coils are close to the equilibrium ones. Using the representation for the conformational tensor $\mathbf{A}=R_0^2\mathbf{I}+\mathbf{A}_1$ where $\mathbf{A}_1$ is small correction and substituting it in Eqs. (6) and (7) one find the stress tensor $\boldsymbol{\Sigma}\simeq G\mathbf{A}_1/R_0^2\simeq\eta\left(\nabla\mathbf{v}+(\nabla\mathbf{v})^{T}\right)$. Hence

$$\Sigma_{zz}-\Sigma_{rr}\simeq 3\eta\dot{\varepsilon},\quad \Sigma_{rr}\simeq-\eta\dot{\varepsilon}. \tag{9a}$$

In the region $\dot{\varepsilon}\tau\simeq 1$ the polymer coils start to unfold and stretch in the flow direction. At that $R_0^2<A_{zz}<L^2$, resulting in stress increase $\boldsymbol{\Sigma}=G\left(\mathbf{A}/R_0^2-\mathbf{I}\right)$ (a strain hardening regime). The incompressibility condition $\nabla\cdot\mathbf{v}=0$ allows finding the radial velocity $\mathrm{v}_r\simeq-\frac{r}{2}\frac{d\mathrm{v}_z}{dz}$, therefore Eq. (7) in the first order yields

$$\tau\mathrm{v}_z\frac{d\Sigma_{zz}}{dz}-2\tau\frac{d\mathrm{v}_z}{dz}\Sigma_{zz}+\Sigma_{zz}\simeq 2\eta\frac{d\mathrm{v}_z}{dz}, \tag{9b}$$

$$\tau\mathrm{v}_z\frac{d\Sigma_{rr}}{dz}+\tau\frac{d\mathrm{v}_z}{dz}\Sigma_{rr}+\Sigma_{rr}\simeq-\eta\frac{d\mathrm{v}_z}{dz}. \tag{9c}$$

Finally at very high strain rates $\dot{\varepsilon}\tau\gg 1$ the chains became nearly fully stretched, $1-\mathrm{tr}\mathbf{A}/L^2\ll 1$, and the normal stress difference and Σ_{rr} read

$$\Sigma_{zz}-\Sigma_{rr}\simeq\eta N\dot{\varepsilon},\quad \Sigma_{rr}\simeq-\frac{2}{3}\eta\dot{\varepsilon}. \tag{9d}$$

C. Charge relaxation equation

The electric field inside the cone and the jet $\mathbf{E}$ induces a current $\mathbf{j}(\mathbf{E})$ which obeys a linear Ohm law $\mathbf{j}=K\mathbf{E}$. The normal component of this current is responsible for charging of the free surface. The charge balance equation on a surface area dA is written as

$$\frac{\partial}{\partial t}(\sigma dA)+\nabla_\tau(\sigma\mathrm{v}_\tau dA)=j_n dA. \tag{10}$$

Here v_τ is the tangential component of the surface velocity, ∇_τ is the gradient along $\boldsymbol{\tau}$, and j_n is a normal to the surface component of the electric current. Taking into account that $\frac{\partial}{\partial t}[dA]=\mathrm{v}_n C dA$ and $dA=2\pi r\sqrt{1+r_z'^2}dz$, we arrive to the following charge balance equation:

$$r\sqrt{1+r_z'^2}\frac{\partial\sigma}{\partial t}+\nabla_\tau\left(r\sqrt{1+r_z'^2}\sigma\mathrm{v}_\tau\right)+r\sqrt{1+r_z'^2}\sigma\mathrm{v}_n C=r\sqrt{1+r_z'^2}j_n. \tag{11a}$$

This equation is simplified in the steady state regime

$$\nabla_\tau (r\sigma \mathrm{v}_\tau) \simeq r j_n. \tag{11b}$$

D. Surface charge density

In what follows we divide the cone-jet pattern in two parts which for convenience will be called a conductive and a convective one. The conductive part is attached directly to the nozzle and has virtually equipotential surface (equilibrium distribution of the surface charges), whereas distribution of the surface charges in the convective part is governed by the flow. Transitions between these parts occurs at $z = 0$, with a transition region having a radius $r(0) = b$ ($b < D$). Thus the conductive region is located at $z < 0$ whereas the convective region at $z > 0$. Note that the $z = 0$ point does not necessarily coincide with the point where cone transforms into jet: indeed, some part of the jet can be conductive as well.

Due to the screening effects the electric current in the conductive region is mainly determined by conductivity, $I \simeq \pi r^2 K E_z$, whereas the current carried by the convective region ($z > 0$) is determined by the convective current $I \simeq 2\pi r\sigma \mathrm{v}_z \simeq \frac{2\sigma Q}{r}$. At $z = 0$ both currents have the same order of magnitude, therefore the surface charge density in the transition region reads

$$\sigma^* \simeq \frac{K E b^3}{Q} \simeq \frac{\varepsilon_0 E b^3}{Q\tau_E}. \tag{12}$$

Here and further on the numerical prefactors are omitted. E is the strength of the electric field inside the transition zone and $\tau_E = \frac{\varepsilon_0}{K}$ is the charge relaxation time (note, it is different from the Maxwell relaxation time $\frac{\varepsilon\varepsilon_0}{K}$ and is taken in such form for convenience). For conductive polymer solutions, this time varies typically inside a broad interval $\tau_E \sim 10^{-10} \div 10^{-5}$ s and is usually smaller than the viscoelastic relaxation time τ, therefore an inequality $\tau_E/\tau \ll 1$ is assumed to be valid.[6] The total electric current which is a sum of the conductive and the convective currents equals approximately

$$I \simeq K E b^2. \tag{13}$$

The charge conservation law $I \simeq K E b^2 \simeq \frac{\sigma Q}{r}$ leads to a simple formula for the surface charge density at $z > 0$

$$\sigma \simeq \frac{K E b^2 r}{Q} = \frac{\sigma^* r}{b}. \tag{14}$$

The surface density of the conductive charges in the conductive region (the contribution of the polarization charges is assumed to be small), i.e., at $z < 0$, obeys an integral equation which follows from the Coulomb's law[27]

$$\frac{\sigma}{2\varepsilon_0} = E_0 \mathbf{e}_z \cdot \mathbf{n} + \frac{1}{4\pi\varepsilon_0} \int\limits_A dA_1 \frac{\sigma(\mathbf{r}_1)(\mathbf{r} - \mathbf{r}_1)\cdot \mathbf{n}}{|\mathbf{r} - \mathbf{r}_1|^3}. \tag{15a}$$

Here the integration $\int\limits_A dA_1$ is performed with respect to $\mathbf{r}_1$ over the free cone-jet surface. This equation is simplified after using a slender body approximation

$$\frac{\sigma(z)}{2\varepsilon_0} = -E_0 r_z' + \frac{1}{2\varepsilon_0} \int\limits_{|s-z| \le r(z)/|r_z'|} ds \frac{\sigma(s) r(s) \left(-r_z'(z-s) + r(z)\right)}{\left((z-s)^2 + r^2(z)\right)^{3/2}}, \tag{15b}$$

where we take into account that the charges, which are arranged inside the interval $|s - z| \le r(z)/|r_z'|$, give the main contribution to the integral and the remaining part does not change this estimation. After using an expansion $\sigma(s)r(s) \simeq \sigma(z)r(z) + (\sigma r)_z'(s - z) + 0.5(\sigma r)_{zz}''(s - z)^2$ and integration, we arrive to the following differential equation:

$$\left[(\sigma r)_z' r_z' + 0.5(\sigma r)_{zz}'' r\right] \ln \frac{1}{|r_z'|} - \varepsilon_0 E_0 r_z' \simeq 0. \tag{16}$$

Solution of this equation which conjugates smoothly with Eq. (14) reads

$$\sigma \simeq \frac{\sigma^* b}{r}. \tag{17}$$

Note that Eq. (17) will fail in the near vicinity of the nozzle.

Finally we estimate the electric field strength E_z inside the cone-jet. The total field in the system is a sum of the field from the electrodes $E_0\mathbf{e}_z$ and the field created by the surface charges $\mathbf{E}_s$, $\mathbf{E}_{tot} = E_0\mathbf{e}_z + \mathbf{E}_s$. Based on a slender body approximation and the electrostatic boundary conditions[27] we can conclude that the tangential component of the electric field is

$$E_z \simeq E_0 + \mathbf{E}_s \cdot \mathbf{e}_z. \tag{18}$$

The term $\mathbf{E}_s \cdot \mathbf{e}_z$ is essentially determined by the charges inside the interval $|s - z| \le r(z)/|r_z'|$ in the vicinity of the point z

$$\mathbf{E}_s \cdot \mathbf{e}_z \simeq -\frac{1}{2\varepsilon_0} \int\limits_{|s-z| \le r(z)/|r_z'|} \frac{\sigma(s) r(s)(s-z)ds}{\left((s-z)^2 + r^2(s)\right)^{3/2}}. \tag{19}$$

Using expansion $r(z) \simeq b + r_z' z$ the integration gives the following electric field strength:

$$E_z \simeq E_0 + \frac{E b^2 r \left|r_z'\right|}{Q\tau_E} \ln \frac{1}{\left|r_z'\right|}. \tag{20}$$

Far away from the transition region, at $z > 0$, $E_z \simeq E_0$. Owing to the screening effects, the electric field inside the conductive region is determined from the electric flux conservation law and can be approximately written as

$$E_z \simeq E \left(\frac{b}{r}\right)^2. \tag{21}$$

Thus the electric field attains the maximum value E in the transition region characterized by the length $\ell \simeq \frac{b}{|r_z'|}$,

$$E \simeq \frac{E_0}{1 - \frac{b^3 |r_z'|}{Q\tau_E}}. \tag{22}$$

Here we omitted the logarithmic term. Qualitatively similar behavior for the electric field has been found in numerical calculations.[12,18,19]

Eq. (20) allows one to distinguish two asymptotic cases. If $\frac{b^3|r_z'|}{Q\tau_E} \ll 1$, the field inside the transition zone approximately coincides with the external one, i.e., $E \simeq E_0$. When $1 - \frac{b^3|r_z'|}{Q\tau_E} \ll 1$, the field is mainly determined by the surface charges and, therefore, the electric current does not depend on the external field strength – the situation which is often encountered in electrospraying[23] but is not typical for electrospinning. Therefore we restrict ourselves to the first case only, i.e., it will be assumed that $E \simeq E_0$. The case $\frac{b^3|r_z'|}{Q\tau_E} > 1$ could imply instability of the cone-jet structure.

III. ELECTROSPINNING REGIMES

In Sec. II, we have formulated the full system of electro-hydrodynamic equations describing the dynamics of a charged viscoelastic jet and calculated the surface density of the conductive charges. In this section we focus on the analyses of the jet shapes and formulate an additional condition which allows finding radius of the jet in the transition region and the electric current carried by the jet. Further on we identify four different regimes A, B, C, and D.

In the regimes A and B the conductive region includes the cone and a part of the jet (we call it a conductive jet) having nearly equipotential surface, whereas charge transport in the rest of the jet is convective (a dielectric jet). Distinction between regimes A and B is made based on the rheological

flow regime. In the regime A the conductive jet operates in the Newtonian mode whereas the regime B is in the strain hardening mode.

In the regimes C and D only the cone has equipotential surface whereas the jet behaves as charged dielectric. The regime C operates in the Newtonian mode and the regime D – in the strain hardening mode.

A. Regimes A and B

First we consider the regimes A and B which can be described based on the following assumptions:

1. The flow inside the cone is small and the structure of the cone is mainly determined by the capillary and ponderomotive force (the normal electric traction)

$$\alpha C \simeq F_n. \tag{23a}$$

   Further on we will neglect contribution of the polarization charges so that $F_n \simeq \frac{\sigma^2}{2\varepsilon_0}$.
2. The shape of the conductive jet is stabilized by the viscoelastic and ponderomotive forces so that Eq. (5) reads

$$r^2 \frac{dF_n}{dz} + \frac{d}{dz}\left[r^2\left(\Sigma_{zz} - \Sigma_{nn}\right)\right] \simeq 0. \tag{23b}$$

3. The shape of the dielectric jet is mainly stabilized by the inertia and the tangential electric traction,

$$\frac{d}{dz}\left[r^2 \rho \mathrm{v}_z^2\right] \simeq \frac{\varepsilon_0 E_0^2 b^2 r^2}{Q\tau_E}. \tag{23c}$$

To ensure a smooth transition between the cone and the conductive jet, an equality of the capillary and viscoelastic terms in Eq. (5) have to be imposed at the junction point

$$\alpha r^2 \frac{dC}{dz} \simeq \frac{d}{dz}\left[r^2\left(\Sigma_{nn} - \Sigma_{zz}\right)\right]. \tag{24a}$$

Using approximation $C = 1/r$ and introducing a tensile force $T \equiv r^2(\Sigma_{zz} - \Sigma_{rr})$, Eq. (24a) is written in a simple form

$$\alpha r_0 \simeq T_0, \tag{24b}$$

where r_0 is the radius and T_0 is the tensile force at the cone-jet crossover. Note Eq. (24b) does not imply a force balance: both forces are directed inside the jet and balanced by the normal electric traction. Equations (23a) and (24b) allow evaluation of the tensile force

$$T_0 \simeq r_0^2 \frac{\sigma^{*2} b^2}{\varepsilon_0 r_0^2} \simeq \frac{\varepsilon_0 E_0^2 b^8}{Q^2 \tau_E^2}. \tag{25}$$

Next, the smoothness of the transition between the conductive jet and the dielectric jet should be taken into account. It implies continuity of the derivatives r_z' of the corresponding jet profiles at $r = b$, i.e.,

$$r'_{z,conductive}(r = b) = r'_{z,dielectric}(r = b). \tag{26}$$

In what follows, we make use of a smooth transition between the normal and the tangential electric tractions on the one hand and the conductive and the convective currents on the other hand to calculate the radius b and the electric current.

The shape of the conductive jet in the regime A is determined by Eq. (A4) and depends on the constant β. The shape of the dielectric jet is given by well known Eq. (A16). First we calculate the

constant β. Based on the general equation for the tensile force $T_0 \simeq r_0^2 (\Sigma_{zz} - \Sigma_{rr}) \simeq -\frac{Q\eta r_z'}{r_0}$, where r_z' is given by Eq. (A5), one gets

$$T_0 \simeq \frac{\varepsilon_0 E_0^2 b^8 \beta}{Q^2 \tau_E^2}. \tag{27}$$

Comparing this formula to Eq. (25) we obtain $\beta = 1$.

The derivative r_z' for the conductive and dielectric jet profiles in the transition region ($r = b$) are given by Eqs. (A5) and (A17), respectively. Substitution of these values in Eq. (26) yields

$$b \simeq \left(\frac{\varepsilon_0 \eta}{K\rho}\right)^{\frac{1}{2}}. \tag{28}$$

The electric current Eq. (13) after elimination of the radius using Eq. (28) reads

$$I \simeq \frac{\eta \varepsilon_0 E_0}{\rho}. \tag{29}$$

Interestingly, in the regime A the radius b does not depend on the electric field strength and the flow rate. Also, the electric current is linearly proportional to the electric field strength, $I \sim E_0$. Moreover it is predicted to be insensitive to flow rate and conductivity – a feature that has been observed in recent experiments.[31]

The radius of the cone-jet transition reads $r_0 \simeq \frac{\varepsilon_0 E_0^2 \tau_E^2 \eta^4}{Q^2 \rho^4 \alpha}$. It decreases with increasing flow rate and at certain moment reaches the conductive-convective jet transition zone radius value, $r_0 = b$. This defines the upper boundary of the regime A and a transition into another regime where no conductive jet is realized, as elaborated in Sec. IV:

$$Q_A^{(+)} = \frac{\eta^{\frac{7}{4}} \varepsilon_0^{\frac{5}{4}} E_0}{\alpha^{\frac{1}{2}} \rho^{\frac{7}{4}} K^{\frac{3}{4}}}, \tag{30}$$

i.e., the regime A is realized at $Q < Q_A^{(+)}$. Another restriction on the regime A is connected with an assumption that the electric field generated by the surface charges in z direction is smaller than the external one, see Eq. (22), i.e., $\frac{b^3 |r_z'|}{Q\tau_E} < 1$, or

$$Q > Q_1 = \frac{\varepsilon_0 E_0^{\frac{1}{2}} \eta^{\frac{5}{4}}}{\rho^{\frac{3}{2}} K^{\frac{3}{4}}}. \tag{31}$$

Finally, with decreasing flow rate the strain rate increases as $\dot{\varepsilon} \simeq \frac{\varepsilon_0 E_0^2 b^6}{Q^2 \tau_E^2 \eta}$ so that at

$$Q = Q_A^{(-)} = \eta \varepsilon_0 E_0 \left(\frac{\tau}{\rho^3 K}\right)^{\frac{1}{2}}, \tag{32}$$

the condition $\dot{\varepsilon}\tau \simeq 1$ becomes fulfilled. The boundary Eq. (32) separates the rheologically Newtonian-like regime A from a strain hardening regime B. Thus, the regime A is realized at $Q > Q_A^{(-)}$. The inequality $Q_A^{(+)} > Q_A^{(-)}$ implying $G^3 \tau \tau_E > \rho \alpha^2$ gives a criterion of the existence of regime A.

Hence, at $Q < Q_A^{(-)}$, the strain hardening regime B is realized. The radius b of the transition zone in this regime is found from the continuity of r_z'. After using Eqs. (A9) and (A17) it is written as

$$b \simeq \left(\frac{Q^2 \rho}{K E_0^2 \tau}\right)^{\frac{1}{4}}. \tag{33}$$

This radius increases with increasing flow rate and decreasing electric field strength. The electric current in the regime B is given by

$$I \simeq \left(\frac{\rho K}{\tau}\right)^{\frac{1}{2}} Q. \tag{34}$$

It is linearly proportional to the flow rate and independent on the electric field. For sufficiently large flow rates such behavior has been observed experimentally.[1] The radius of the cone-jet transition follows from Eqs. (24b), (25), and (33) and reads

$$r_0 \simeq \frac{\rho^2 Q^2}{\varepsilon_0 E_0^2 \tau^2 \alpha}. \tag{35}$$

Restrictions on the strain hardening regime B are determined by inequalities $r_0 > b$ and $\frac{b^3|r_z'|}{Q\tau_E} \simeq \frac{b^6}{Q^2\tau\tau_E} < 1$, leading to the boundaries

$$Q > Q_B^{(-)} = \frac{\alpha^{\frac{2}{3}}\tau^{\frac{7}{6}}\varepsilon_0^{\frac{2}{3}}E_0}{\rho^{\frac{7}{6}}K^{\frac{1}{6}}}, \tag{36a}$$

$$Q < Q_2 = \frac{\varepsilon_0 E_0^3 \tau^{\frac{5}{2}} K^{\frac{1}{2}}}{\rho^{\frac{3}{2}}}. \tag{36b}$$

B. Regimes C and D

These regimes are realized when conductive jet does not appear and a transition from conductive to convective current occurs in the cone-jet transition region. The following assumptions define those regimes:

1. Similar to the regimes A and B, the structure of the cone is mainly determined by the capillary force and ponderomotive force, i.e., $\alpha C \simeq F_n$.
2. The structure of the jet is governed by viscoelastic, inertial and tangential electric forces,

$$\frac{d}{dz}\left[r^2\left(\frac{\rho \mathrm{v}_z^2}{2} + \Sigma_{rr} - \Sigma_{zz}\right)\right] \simeq \frac{\varepsilon_0 E_0^2 b^2 r^2}{Q\tau_E}. \tag{37}$$

In order to find the jet profiles, which are solutions of Eq. (37), the initial radius b and the initial derivative r_z' in the cone-jet transition region should be defined. Let us formulate the conditions which allow finding these values. The smoothness of the cone-jet transition region implies (see Eq. (5))

$$\alpha r^2 \frac{dC}{dz} \simeq \frac{d}{dz}\left[r^2\left(\frac{\rho \mathrm{v}_z^2}{2} + \Sigma_{rr} - \Sigma_{zz}\right)\right]. \tag{38}$$

Assuming $C \simeq 1/r$, after integration one gets the following scaling relations:

$$\alpha b \simeq T_0 \simeq \frac{\varepsilon_0 E_0^2 b^8}{Q^2 \tau_E^2}, \tag{39}$$

where $T_0 \simeq b^2(\Sigma_{zz} - \Sigma_{rr})$. Here an equivalence of the capillary and ponderomotive forces has been used and inertia has been omitted in the cone-jet transition region.

The shapes of the jet in the regime C are presented in the Appendix, Eq. (A11). The radius b and the derivative r_z' at the cone-jet transition region are obtained from Eq. (39) using $T_0 \simeq -\frac{3Q\eta r_z'}{b}$

$$b \simeq \left(\frac{\varepsilon_0 \alpha Q^2}{E_0^2 K^2}\right)^{\frac{1}{7}}, \quad r_z'(z=0) \simeq -\frac{\alpha b^2}{Q\eta}. \tag{40}$$

The electric current reads

$$I \simeq \left(\alpha^2 \varepsilon_0^2 E_0^3 Q^4 K^3\right)^{\frac{1}{7}}. \tag{41}$$

Note, that this scaling behavior is similar to the results obtained by Reznik and Zussman[12] in what they called a capillary-dominated regime. The initial conditions Eq. (40) uniquely determine the shape of the jet which is a solution of the second order differential equation (A10).

Inertia becomes dominant in the transition region when $r_z'(z=0) \simeq -\frac{\alpha b^2}{Q\eta} \simeq -\frac{\varepsilon_0 E_0^2 b^7}{\rho Q^3 \tau_E}$, or at

$$Q = Q_A^{(+)} \simeq \frac{\eta^{\frac{7}{4}} \varepsilon_0^{\frac{5}{4}} E_0}{\alpha^{\frac{1}{2}} \rho^{\frac{7}{4}} K^{\frac{3}{4}}}, \tag{42}$$

i.e., the regime C is realized at $Q > Q_A^{(+)}$. Thus $Q_A^{(+)}$ is a boundary between the regimes A and C. An additional restriction on the regime C is due to the electric field induced by the surface charges, which should not exceed the external one, see Eq. (22), i.e., $\frac{b^3|r_z'|}{Q\tau_E} < 1$, or

$$Q > Q_3 = \frac{\alpha^3}{\eta^{\frac{7}{4}} \varepsilon_0^{\frac{1}{2}} E_0^{\frac{5}{2}} K^{\frac{3}{4}}}. \tag{43}$$

With decreasing flow rate at some point the condition $\dot{\varepsilon}\tau \simeq 1$ is fulfilled. It implies onset of the strain hardening mode. The corresponding transition occurs when the flow rate reads

$$Q = Q_C^{(-)} \simeq \frac{\alpha^3 K E_0}{\varepsilon_0^{\frac{1}{2}} G^{\frac{7}{2}}}. \tag{44}$$

It gives another lower boundary for the regime C. Inequality $Q_C^{(-)} < Q_A^{(+)}$ implies $G^3 \tau \tau_E > \rho\alpha^2$.

The case $Q < Q_C^{(-)}$, corresponding to the strain hardening mode, is attributed to the regime D. According to Eq. (39) the radius of the transition region in the regime D coincides with that in the regime C, i.e., $b \simeq \left(\frac{Q^2\tau_E^2\alpha}{\varepsilon_0 E_0^2}\right)^{\frac{1}{7}}$ and the tensile force is given by $T_0 \simeq \frac{\varepsilon_0 E_0^2 b^8}{Q^2\tau_E^2}$. Formation of the thinning jet is possible if simultaneously $T_0 > \frac{\rho v_z^2 b^2}{2}$ and $T_0 > 2T^* \simeq \frac{\varepsilon_0 E_0^2 b^2 \tau}{\tau_E}$ (see Eq. (A19b)). The last inequality is written as $\frac{b^6}{Q^2\tau\tau_E} > 1$. On the other hand Eq. (A20) gives $r_z'(z=0) \simeq -\frac{b^3}{Q\tau}$, therefore an inequality $\frac{b^3|r_z'|}{Q\tau_E} \simeq \frac{b^6}{Q^2\tau\tau_E} < 1$ has to be fulfilled. This brings us to a contradiction implying that stable jetting is impossible in the regime D.

IV. STABILITY OF THE CONE – JET MODE AND THE OPERATING WINDOW

In this section we address the operating window where a stable jetting mode can be realized. In practice, a steady spinning region in the (E_0, Q) plane is rather restricted: for each value of the external electric field, a maximum and a minimum pump flow rates exist, beyond which no stable steady spinning is possible.[6,22] In what follows, two cases corresponding to $G^3\tau\tau_E < \rho\alpha^2$, Fig. 2(a), and $G^3\tau\tau_E > \rho\alpha^2$, Fig. 2(b) are identified.

In Figure 2 we introduce the following electric field values:

$$E^* = \frac{G}{\eta^{\frac{1}{2}} K^{\frac{1}{2}}}, \quad E_1 = \frac{\alpha^{\frac{1}{3}} \rho^{\frac{1}{6}}}{\varepsilon_0^{\frac{1}{6}} \tau^{\frac{2}{3}} K^{\frac{1}{3}}}, \quad E_2 = \frac{\alpha\rho^{\frac{1}{2}}}{\eta\varepsilon_0^{\frac{1}{2}}}, \quad E_3 = \frac{\alpha^{\frac{3}{2}} \rho^{\frac{3}{4}} K^{\frac{1}{4}}}{\varepsilon_0^{\frac{3}{4}} \tau^{\frac{5}{4}} G^{\frac{7}{4}}}. \tag{45}$$

When $G^3\tau\tau_E < \rho\alpha^2$, only the regimes B, C, and D are identified. As has been shown above, the regime D is unstable and this kind of instability can be responsible for the minimal flow rate at which intermittent jet is observed.[5] After using Eqs. (8) and (40), the strain rate in the regime C is given by $\dot{\varepsilon} \simeq \frac{\alpha b}{\eta}$. It is inversely proportional to the breakage time of a filament of radius b, $\tau_\eta \simeq \frac{\eta}{\alpha b}$, when the instability is governed by viscous and capillary forces.[32] Thus one could expect that the regime C or part of this regime is unstable. We do not consider this point in the present work. One can suggest that dripping cone is related to this kind of instability. The flow rates corresponding to the characteristic fields E^* and E_1 are given by $Q(E^*) \simeq \frac{\alpha^3}{G^3\tau^{\frac{1}{2}}\tau_E^{\frac{1}{2}}}$ and $Q(E_1) \simeq \frac{\alpha\tau^{\frac{1}{2}}\tau_E^{\frac{1}{2}}}{\rho}$. According to Eqs. (36a), (36b), and (44) the area of the regime B increases with increasing conductivity.

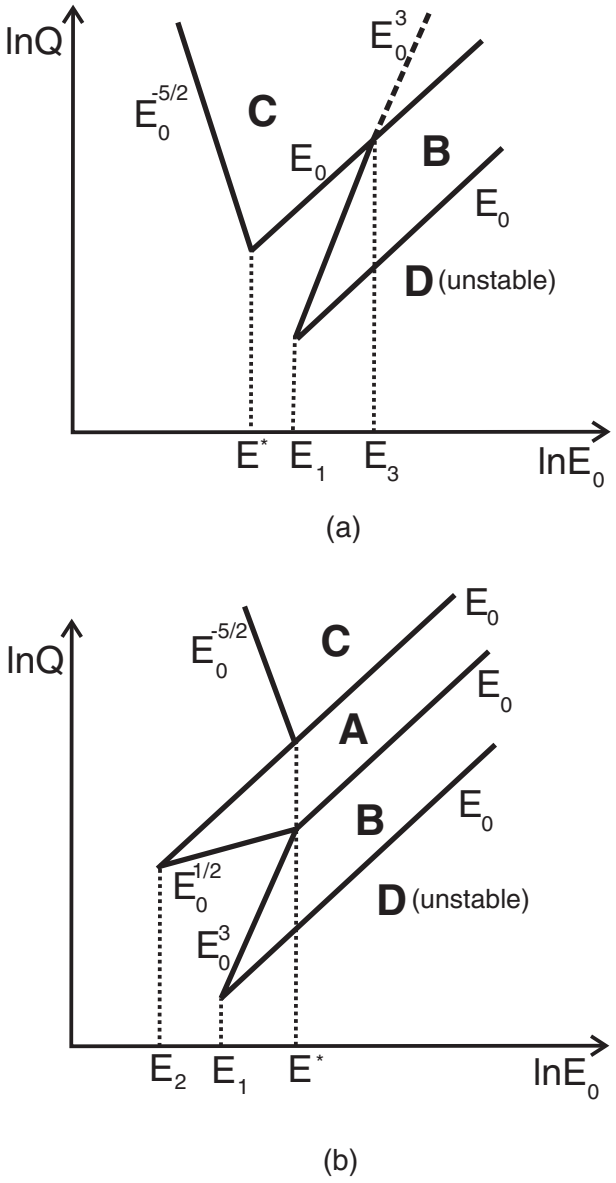

FIG. 2. Schematic diagrams demonstrating location of different electrospinning regimes (the operating window). Details are in the text.

In the case of $G^3\tau\tau_E > \rho\alpha^2$ all regimes A, B, C, and D are possible. The additional regime A is restricted by the boundaries from Eqs. (30), (31), and (32). With increasing conductivity this regime moves to the region of low flow rates.

The operating window could be restricted at strong electric fields when the multi-jet modes appear and at week electric fields when effect of the surface charges becomes dominant. However, to reveal the single-jet/multi-jet boundary and the effect of surface charges, an additional analysis is needed, which is beyond our present scope.

Other types of instabilities such as the bending (whipping) instability and the capillary instability related to the jet dynamics have been discussed in Refs. 17, 33, and 35 and are out of the scope of this paper. The polymer elasticity has an essential influence on the Rayleigh instability in the jet region and on the transition to the beads-on-string jet structure, particularly the Rayleigh instability can be arrested if the elongational stress exceeds some critical value.[33–35]

V. CONCLUDING REMARKS

In the present paper analysis of the different spinning regimes has been performed and an operating window of the electrospinning process has been predicted. We base our approach on rigorous electro-hydrodynamic equations, formulated within the leaky dielectric model[13] and complemented by a constitutive equation of the polymer liquid. The viscoelastic effects are incorporated by an appropriate choice of the constitutive model – the FENE-P model is used to incorporate the effects of chain stretch on the spinnability.[25]

By analysing the electro-hydrodynamics in the jet region we found that both the normal electric traction and tangential electric traction manifest as driving forces of the flow inside the jet. It allows predicting existence of different jet profile types. The inverse square root profiles $r(z) \sim z^{-1/2}$ observed in experiment[27–29] are shown to be the result of the strain hardening mode. Inertial effects lead to a well known[27] scaling $r(z) \sim z^{-1/4}$. Additionally the exponential and double exponential decay of the jet profile are predicted.

Based on the momentum and electric field equations we examined four electrospinning regimes. Measurable quantities, such as the jet radius and the electric current, are calculated for three of them. The regime A in which the jet first is driven by the normal electric force and then by the tangential electric force operates in the Newtonian mode. At that the current scales as $I \sim \eta E_0$, i.e., linearly proportional the electric field. The jet dynamics in the regime B is driven by the same forces as in the regime A but operates in the strain hardening mode. It gives the linear relation between the electric current and the flow rate $I \sim (K/\tau)^{\frac{1}{2}} Q$. In the regimes C and D the jet is driven only by the tangential electric traction: at that the regime D operates in the strain hardening mode and is unstable due to "overcharging" of the jet surface and the regime C operates in the Newtonian mode and could be capillary unstable.

In experiment, quite often a distinction is made between "high" and "low" conductivity polymeric solutions, with the first ones being the most interesting as they allow to produce the thinnest fibers.[6] Note, that our theory predicts different type of operating windows for those two types of solution, as the choice between Figures 2(a) and 2(b) is made based, among other parameters, on conductivity: highly conductive liquids are expected to show the behavior represented by Figure 2(a). Hence, from a practical point of view, it is instructive to estimate the characteristic values of the parameters for the typical representatives "high" and "low" conductivity solutions. Here we base our estimations on the experimental results presented by Wang *et al.*,[6] who systematically studied polymers and solvents of different chemical nature.

Polyamide 6 (PA6) in formic acid (FA) is probably the most industrially relevant representative of the "highly conductive" solutions.[36] It features very high conductivity and allows to produce nanofibers down to sub-100 nm range. An example of low conductivity solution is poly(D-L-lactic acid) (PLA) dissolved in dimethylformamide (DMF). Somewhat intermediate conductivities are detected, e.g., for polyacrylonitrile (PAN) in DMF system. The properties of all three examples, extracted from Ref. 6 are listed in Table I. Parameters such elastic modulus $G = \eta/\tau$ and charge relaxation time $\tau_E = \frac{\varepsilon_0}{K}$ can be estimated from those data as well; we also assume the densities to be around 1000 kg/m^3.

It is easy to check that inequality $\frac{G^3 \tau \tau_E}{\rho \alpha^2} < 1$ is valid for all solutions PA6/FA, PAN/DMF, and PLA/DMF, therefore these systems fall into diagram of Figure 2(a) and operate in the regime B. The radius of the jet b estimated from Eq. (33) is presented in the last column of the Table I. The results are in good agreement with experiment.[6]

TABLE I. Parameters of three representative solutions of different conductivities. Values are from Wang *et al.*[6] except the last column, calculated from Eq. (33).

	η (Pa s)	τ (ms)	K (mS/cm)	E_0 (kV/m)	Q (ml/h)	d_j (μm)	$2b$ (μm)
PA6/FA	0.21	0.4	4.3	1700	0.1	...	0.4
PAN/DMF	0.17	2	0.036	280	0.3	3.3	3.8
PLA/DMF	3.52	2	0.0064	300	1	6.4	10

Unfortunately, most of the data available in the literature disallows a detailed comparison of the present theoretical predictions to experiment. However, let us emphasize that the numerical values of the typical electric field values (45) are well in the range of the practically observed ones. For example, for PA6/FA solutions, Eqs. (45) predict $E^* = 3 \times 10^3$ V/m and $E_1 = 2 \times 10^4$ V/m.

Note that the analysis presented here omits certain details, which might be important in experiments. First of all, the multi-jet operating mode as well as the polarization charges has been neglected. One can expect multi-jetting to become important, especially at high fields or large nozzle diameters, when the typical length scale of unstable surface perturbations becomes smaller than the drop diameter.[37,38] Additionally, the exact details of the external field configuration have not been considered and homogeneous external field strength E_0 has been assumed. At the same time, in practice, long protruding needles are often used, leading to strong field inhomogeneities. In such a situation, the field strength parameter E_0 used in our approach is to be associated with the typical vertical component of the field in the vicinity of the needle tip and not with the electric voltage divided by the inter-electrode distance, as is done sometimes in the literature.

ACKNOWLEDGMENTS

A. Subbotin acknowledges partial support from the Russian Ministry of Education and Science, Contract No. 8534, September 07, 2012.

APPENDIX: THE JET PROFILES

Let us begin by considering a conductive jet which is governed by the viscous and ponderomotive forces. After using formula $\Sigma_{zz} - \Sigma_{nn} \simeq 3\eta\dot{\varepsilon} \simeq -\frac{6Q\eta r'_z}{\pi r^3}$, Eq. (23b) is written as

$$r^2 \frac{dF_n}{dz} - \frac{d}{dz}\left[\frac{6Q\eta r'_z}{\pi r}\right] \simeq 0, \tag{A1}$$

where the ponderomotive force F_n approximately reads

$$F_n \simeq \frac{\sigma^{*2} b^2}{2\varepsilon_0 r^2} \simeq \frac{\varepsilon_0 E_0^2 b^8}{2(Q\tau_E)^2 r^2}. \tag{A2}$$

Substitution of Eq. (A2) in Eq. (A1) yields

$$\frac{\varepsilon_0 E_0^2 b^8}{(Q\tau_E)^2}\frac{r'_z}{r} + \frac{6Q\eta}{\pi}\frac{d}{dz}\left[\frac{r'_z}{r}\right] \simeq 0. \tag{A3}$$

Solutions of the last equation are given by

$$r(z) = b\exp\left[\beta\left(e^{-Az} - 1\right)\right], \quad A = \frac{\pi\varepsilon_0 E_0^2 b^8}{6Q^3\eta\tau_E^2}, \tag{A4}$$

with $r(z = 0) = b$ and β is an integration constant. It is interesting to note that asymptotically ($z \to \infty$) the shape of the conductive jet transforms to a cylinder of the radius $r(z \to \infty) = be^{-\beta}$. The derivative r'_z at $z = 0$ reads

$$r'_z = -rA\beta\left(1 + \ln\frac{r}{b}\right) = -\frac{\pi\varepsilon_0 E_0^2 b^9 \beta}{6Q^3\eta\tau_E^2} \tag{A5}$$

and the strain rate $\dot{\varepsilon} \simeq -\frac{Qr'_z}{r^3} \sim \frac{1}{r^2}$ attains maximum at the cone-jet crossover.

To proceed with the strain hardening mode, first we introduce the following notations: $T(r) \simeq r^2\Sigma_{zz}$ and $\psi(r) = r'_z$. In that case Eqs. (23b) and (9b) read

$$\frac{\varepsilon_0 E_0^2 b^8}{(Q\tau_E)^2 r} - \frac{dT}{dr} \simeq 0, \tag{A6a}$$

$$\frac{Q\tau\psi(r)}{r^3}\left(r\frac{dT}{dr} + 2T\right) + T = 0. \tag{A6b}$$

Solution of Eq. (A6a) is written as

$$T = T_0 + \frac{\varepsilon_0 E_0^2 b^8}{Q^2 \tau_E^2} \ln \frac{r_0}{r}. \tag{A7}$$

Here $T_0 \simeq \frac{\varepsilon_0 E_0^2 b^8}{Q^2 \tau_E^2}$ is the tensile force and r_0 is the radius of the cone at the cone-jet crossover. Taking into account that $r_0 > b$ the jet profile is approximately written as

$$r(z) \simeq b \left(1 + \frac{b^2 z}{Q\tau}\right)^{-\frac{1}{2}}. \tag{A8}$$

The derivative r_z' at $z = 0$ is given by

$$r_z'(z=0) \simeq -\frac{r^3}{Q\tau} = -\frac{b^3}{Q\tau}. \tag{A9}$$

The scaling behavior $r(z) \sim z^{-1/2}$ has been both found in experiments[29,30] and predicted theoretically using different arguments.[29]

Next we address a jet which is governed by viscous and tangential electric forces. The momentum Eq. (37) is written as

$$\frac{6Q\eta}{\pi} \frac{d}{dz}\left[\frac{r_z'}{r}\right] \simeq \frac{K E_0^2 b^2 r^2}{Q}. \tag{A10}$$

Solution of this differential equation depends on the initial radius b and the initial value of the derivative $r_z'(z=0) = -w$. It can be solved analytically if we introduce a new function $f(r) \equiv \frac{r_z'}{r}$ so that (A10) is rewritten as $ff_r' = 2Br$ with $B = \frac{\pi K E_0^2 b^6}{12 Q^2 \eta}$. A general solution of this equation is given by

$$z(r) = \frac{b}{2} \int_{r^2/b^2}^{1} \frac{dx}{x\sqrt{w^2 + B(x-1)}}. \tag{A11}$$

The derivative r_z' and the strain rate read

$$r_z' = -\frac{r}{b}\sqrt{w^2 + B\left(\frac{r^2}{b^2} - 1\right)}, \tag{A12a}$$

$$\dot{\varepsilon} \simeq \frac{Q}{br^2}\sqrt{w^2 + B\left(\frac{r^2}{b^2} - 1\right)}. \tag{A12b}$$

Later on we consider the limiting cases. If $w^2 \gg B$ Eq. (A11) is simplified,

$$r(z) \simeq b \exp\left(-\frac{wz}{b}\right). \tag{A13a}$$

If $w^2 = B$ we arrive to well known result[12,24]

$$r(z) \simeq b \left(1 + \frac{wz}{b}\right)^{-1}. \tag{A13b}$$

Finally at $w^2 < B$ the jet has finite length, $z_{\max} = z(r_{\min})$, where the minimal radius $r_{\min}$ is obtained from the following equation:

$$w^2 + B\left(\frac{r_{\min}^2}{b^2} - 1\right) = 0. \tag{A14}$$

At that $r_z'(z = z_{\max}) = 0$, therefore the strain rate $\dot{\varepsilon} = 0$.

Analysis shows that the strain rate $\dot{\varepsilon}$ increases with jet thinning at $w^2 \geq B$ and decreases at $w^2 < B$. Therefore in the first case one could expect transition to the strain hardening mode when $\dot{\varepsilon}\tau \simeq 1$.

In the above analysis we do not take into account the inertial effects. The momentum equation (37) at $\rho v_z^2 \gg \Sigma_{zz} - \Sigma_{nn}$ is a first order differential equation

$$\frac{\rho Q^2}{\pi^2}\frac{d}{dz}\left[\frac{1}{r^2}\right] \simeq \frac{\varepsilon_0 E_0^2 b^2 r^2}{Q\tau_E}. \tag{A15}$$

Its solution defined by the initial radius $r(z=0) = b$ reads

$$r(z) \simeq b\left(1 + \frac{2\pi^2 \varepsilon_0 E_0^2 b^6 z}{\rho Q^3 \tau_E}\right)^{-\frac{1}{4}}. \tag{A16}$$

The asymptotic behavior $r(z) \sim z^{-1/4}$ has been first predicted by Kirichenko *et al.*[28] The initial derivative value reads

$$r_z' \simeq -\frac{\varepsilon_0 E_0^2 b^2 r^5}{\rho Q^3 \tau_E} = -\frac{\varepsilon_0 E_0^2 b^7}{\rho Q^3 \tau_E}. \tag{A17}$$

Finally we consider the strain hardening mode assuming $\dot{\varepsilon}\tau \simeq 1$ and $G < \Sigma_{zz} < GN$. After introduction of $T(r) = r^2\Sigma_{zz}$, $T_0 = b^2\Sigma_0$, $T^* = K E_0^2 b^2 \tau$, and $\psi(r) = r_z'$ the momentum equation (37) and the constitutive equation (9b) are written as

$$\psi(r)\left(\frac{\rho Q^2}{\pi^2 r^3} + \frac{dT}{dr}\right) \simeq -\frac{2T^* r^2}{Q\tau}, \tag{A18a}$$

$$\frac{Q\tau\psi(r)}{r^3}\left(r\frac{dT}{dr} + 2T\right) + T = -\frac{6Q\eta\psi(r)}{\pi r}. \tag{A18b}$$

After some calculations these equations are rewritten in the form

$$\frac{dT}{dr}\left(1 - \frac{2T^*}{T}\right) \simeq \frac{2T^*}{r}\left(2 + \frac{6Gr^2}{\pi T^*} - \frac{\rho Q^2}{2\pi^2 r^2 T^*}\right), \tag{A19a}$$

$$\frac{dr}{dz} \simeq -\frac{r^3}{2Q\tau}\left(1 - \frac{2T^*}{T}\right)\left(1 + \frac{3Gr^2}{\pi T} - \frac{\rho Q^2}{2\pi^2 r^2 T}\right)^{-1}. \tag{A19b}$$

These equations can be simplified in the two limiting cases, namely when inertia is dominant and when inertia is small. Further on, the term $\frac{3Gr^2}{\pi T} < 1$ can be omitted. In the first case two conditions $\frac{\rho Q^2}{2\pi^2 r^2 T} > 1$ and $\frac{2T^*}{T} > 1$ ensure the solution of (A19b) yields a thinning jet. It easy to see that Eq. (A19b) in the first order gives the profile Eq. (A16).

In the second case thinning jet solution appears when $\frac{\rho Q^2}{2\pi^2 r^2 T} < 1$ and $\frac{2T^*}{T} < 1$. Equation (A19b) approximately reads

$$\frac{dr}{dz} \simeq -\frac{r^3}{2Q\tau}\left(1 - \frac{2T^*}{T}\right) \simeq -\frac{r^3}{2Q\tau}. \tag{A20}$$

From the last equation the jet profile is obtained

$$r(z) \simeq b\left(1 + \frac{b^2 z}{Q\tau}\right)^{-\frac{1}{2}}. \tag{A21}$$

Note, when the tensile force $T = 2T^*$, the derivative $r_z' = 0$.

[1] Y. M. Shin, M. M. Hohman, M. P. Brenner, and G. C. Rutledge, "Experimental characterization of electrospinning: the electrically forced jet and instabilities" Polymer **42**, 9955 (2001).
[2] S. A. Theron, E. Zussman, and A. L. Yarin, "Experimental investigation of the governing parameters in the electrospinning of polymer solutions," Polymer **45**, 2017 (2004).
[3] Z.-M. Huang, Y.-Z. Zhang, M. Kotaki, and S. Ramakrishna, "A review on polymer nanofibers by electrospinning and their applications in nanocomposites," Compos. Sci. Technol. **63**, 2223 (2003).
[4] P. Heikkilä and A. Harlin, "Parameter study of electrospinning of polyamide-6," Eur. Polym. J. **44**, 3067 (2008).
[5] D. H. Reneker, A. L. Yarin, E. Zussman, and H. Xu, "Electrospinning of nanofibers from polymer solutions and melts," Adv. Appl. Mech. **41**, 43 (2007).

[6] C. Wang, Y.-W. Cheng, C.-H. Hsu, H.-C. Chien, and S.-Y. J. Tsou, "How to manipulate the electrospinning jet with controlled properties to obtain uniform fibers with the smallest diameter? – a brief discussion of solution electrospinning process," Polym. Res. **18**, 111 (2011).
[7] A. Formhals, "Process and apparatus for preparing artificial threads," U.S. patent 1,975,504 (Oct. 2, 1934).
[8] A. L. Yarin and E. Zussman, "Upward needleless electrospinning of multiple nanofibers," Polymer **45**, 2977 (2004).
[9] M. Cloupeau and B. Prunet-Foch, "Electrostatic spraying of liquids in cone-jet mode," J. Electrost. **22**, 135 (1989).
[10] F. J. Higuera, "Flow rate and electric current emitted by a Taylor cone," J. Fluid Mech. **484**, 303 (2003).
[11] A. M. Ganan-Calvo, "On the general scaling theory for electrospraying," J. Fluid Mech. **507**, 203 (2004).
[12] S. N. Reznik and E. Zussman, "Capillary-dominated electrified jets of a viscous leaky dielectric liquid," Phys. Rev. E **81**, 026313 (2010).
[13] R. Collins, M. Harris, and O. Basaran, "Breakup of electrified jets," J. Fluid Mech. **588**, 75 (2007).
[14] D. A. Saville, "Electrohydrodynamics: The Taylor-Melcher leaky dielectric model," Annu. Rev. Fluid Mech. **29**, 27 (1997).
[15] F. Yan, B. Farouk, and F. Ko, "Numerical modeling of an electrostatically driven liquid meniscus in the cone-jet mode," J. Aerosol Sci. **34**, 99 (2003).
[16] R. T. Collins, J. J. Jones, M. T. Harris, and O. A. Basaran, "Electrohydrodynamic tip streaming and emission of charged drops from liquid cones," Nat. Phys. **4**, 149 (2008).
[17] M. M. Hohman, Y. M. Shin, G. C. Rutledge, and M. P. Brenner, "Electrospinning and electrically forced jets. I. Stability theory," Phys. Fluids **13**, 2201 (2001).
[18] M. M. Hohman, Y. M. Shin, G. C. Rutledge, and M. P. Brenner, "Electrospinning and electrically forced jets. II. Applications," Phys. Fluids **13**, 2221 (2001).
[19] J. J. Feng, "The stretching of an electrified non-newtonian jet: A model for electrospinning," Phys. Fluids **14**, 3912 (2002).
[20] J. J. Feng, "Stretching of a straight charged viscoelastic jet," J. Non-Newtonian Fluid Mech. **116**, 55 (2003).
[21] C. P. Carroll and Y. L. Joo, "Electrospinning of viscoelastic Boger fluids: Modeling and experiments," Phys. Fluids **18**, 053102 (2006).
[22] J. Fernández de la Mora, "The fluid dynamics of Taylor cones," Annu. Rev. Fluid Mech. **39**, 217 (2007).
[23] J. Fernández de la Mora and I. G. Loscertales, "The current emitted by highly conducting Taylor cones," J. Fluid Mech. **260**, 155 (1994).
[24] F. G. Higuera, "Stationary viscosity-dominated electrified capillary jets," J. Fluid Mech. **558**, 143 (2006).
[25] J. M. Rallison and E. J. Hinch, "Do we understand the physics of the constitutive equation?," J. Non-Newtonian Fluid Mech. **29**, 37 (1988).
[26] R. B. Bird, R. C. Armstrong, and O. Hassager, *Dynamics of Polymeric Liquids* (Wiley, New York, 1987), Vol. 1.
[27] L. D. Landau, E. M. Lifshitz, and L. P. Pitaevskii, *Electrodynamics of Continuous Media* (Pergamon Press, Oxford, 1984).
[28] N. Kirichenko, I. V. Petryanov-Sokolov, N. N. Suprun, and A. A. Shutov, "Asymptotic radius of a slightly conducting liquid jet in an electric field," Sov. Phys. Dokl. **31**, 611 (1986).
[29] M. E. Helgeson, K. N. Grammatikos, J. M. Deitzel, and N. J. Wagner, "Theory and kinematic measurements of the mechanics of stable electrospun polymer jets," Polymer **49**, 2924, (2008).
[30] I. Greenfeld, K. Fezzaa, M. H. Rafailovich, and E. Zussman "Fast x-ray phase-contrast imaging of electrospinning polymer jets: Measurements of radius, velocity, and concentration," Macromolecules **45**, 3616 (2012).
[31] P. K. Bhattacharjee, T. M. Schneider, M. P. Brenner, G. H. McKinley, and G. C. Rutledge, "On the measured current in electrospinning," J. Appl. Phys. **107**, 044306 (2010).
[32] S. Chandrasekhar, *Hydrodynamic and Hydromagnetic Stability* (Dover Publications, New York, 1981).
[33] J. H. Yu, S. V. Fridrikh, and G. C. Rutledge, "The role of elasticity in the formation of electrospun fibers," Polymer **47**, 4789 (2006).
[34] C. P. Carroll and Y. L. Joo, "Axisymmetric instabilities of electrically driven viscoelastic jets," J. Non-Newtonian Fluid Mech. **153**, 130 (2008).
[35] H.-C. Chang, E. A. Demekhin, and E. Kalaidin, "Iterated stretching of viscoelastic jets," Phys. Fluids **11**, 1717 (1999).
[36] D. Cho, E. Zhmayev, and Y. L. Joo, "Structural studies of electrospun nylon 6 fibers from solution and melt," Polymer **52**, 4600 (2011).
[37] S. Martin, A. Perea, P. L. Garcia-Ybarra, and J. L. Castillo, "Effect of the collector voltage on the stability of the cone-jet mode in electrohydrodynamic spraying," J. Aerosol Sci. **46**, 53 (2012).
[38] T. Miloh, B. Spivak, and A. L. Yarin, "Needleless electrospinning: Electrically driven instability and multiple jetting from the free surface of a spherical liquid layer," J. Appl. Phys. **106**, 114910 (2009).